Modeling of Explosively Driven Dispersion: Application to the Fukushima Daiichi Accident

Charline Fouchier, Joseph Shepherd
California Institute of Technology
Pasadena, California, USA

1 Introduction

On March 11, 2011, the earthquakes and tsunamis off the northeast coast of Japan resulted in the catastrophic failure of the engineering safety systems and the destruction of the cores and rupture of the containment systems in reactor units 1, 2, 3, and 4 of the Fukushima Daiichi Nuclear Power Plant (NPP). Numerous investigations were performed, and multiple reports on the accidents have been published (a selection is given in Table 1.1 of the National Research Council report NAS, 2014).

One consequence of the destruction of the reactor cores was the production of large quantities of combustible gas, hydrogen from the oxidation of hot metal in the core, and carbon monoxide from molten core-concrete interactions. The combustible gas exploded in units 1, 3 and 4, causing significant damage to the structures and systems at the site. The explosions in Fukushima Daiichi Unit 1 (1F1) on March 12, 2011, and Unit 3 (1F3) on March 14, 2011, were documented in video recordings made by a camera operated by Fukushima Central Television (FCT). These video recordings were broadcast worldwide, contributing substantially to safety concerns and reactions at the time and continue to be scrutinized to this day. These images also form a unique record of an unprecedented event and provide evidence that could potentially be used to quantify amount and explosion mode of the combustible gases.

The present study is a contribution to the extensive literature on the forensic analysis (Rempe et al 2017) of Fukushima explosions. Our work is based on using the plumes observed in the FCT images. These images were first analyzed by Tsuruda (2013) to create space-time diagrams of the spreading of the gas cloud. From these, he proposed possible explanations for the visual appearance and nature of the explosions. Yanez et al. (2015) and Kuznetsov et al. (2015) developed likely explosion scenarios informed by the video images, computational analyses, and experimental data on hydrogen combustion. Luangdilok (2020) draws conclusions about the combustion mode on the basis of the extent of damage, debris cloud size and motion as well as the luminosity. His conclusions on the mass of hydrogen involved are based on the analogy of the plume to a fireball from a hydrocarbon vapor cloud explosion.

Our approach is to examine these plumes from the perspective of plume physics and the phenomenology of explosively driven dispersion. We offer some new insights about the nature of the plumes by coupling FCT image analysis with recent scaling results that include both the effects of buoyancy and initial flow inertia. These analyses suggest new lines of inquiry for efforts that seek to use the plume data to determine the energy and rate of energy release of the underlying explosions.

Correspondence to: charline@caltech.edu

2 Image Characteristics and Processing

Yuji Terahsima (2014) of FCT provided a WMV format file containing the images of the 1F1 and 1F3 explosions. The original images were recorded in standard definition (SD) NTSC format 480i (display resolution of 640 px wide and 480 px high after horizontal scaling) in interlaced fields (59.94 fields per second) and up converted to high definition (HD) NTSC format 1080p (1930 px wide, 1080 px high) in RGB24 format, 29.97 progressive frames per second. The difference between progressive and interlaced images is important because some of the images previously used by investigators were obtained from the broadcast outlets that used image conversion methods and processing on original interlaced images to double the framing rate effectively. This can only be identified by accessing the time code information supplied on the file provided by FCT.

Figure 1: View of Fukushima Daiichi nuclear power plant from the FCT camera with key feature identification. Raw image of the entire frame immediately prior to the explosion event in 1F1 on March 12, 2011.

An image of the entire view captured by the FCT camera is shown in Figure 1. The landscape and towns southwest of the NPP are visible in the foreground and displayed along the shoreline (about 3 km are visible) at the mid-height of the frame. The black bars result from the up-conversion and the difference in aspect ratio (4:3) of SD vs HD (16:9) frames. Another consequence of the up conversion from 480i to 1080p is the interpolation of the original 307,200 pixels onto multiple pixels of the 2,084,400 pixels of the 1080p images. Each pixel in the original 480i image is mapped onto an approximately 2x3 rectangle of pixels in the 1080p image, giving the image a grainy quality when viewed at high magnification. The time encoding (TCR) is shown on the lower portion of the frame in the SMPTE format Hour:Minute:Second:Frame with the frame counter running from 0 to 29 with 1/29.97 = 0.03337 s between successive frames. Prominent features of the NPP are labeled.

The camera was located about 10 km SW of the NPP on a hill (Tsuruda, 2013) and viewed the north-south axis of the site obliquely. The viewing angle, estimated by using the location of major features such as the exhaust stacks, has been estimated at 28.6◦ relative to the alignment of reactor buildings 1-4, which are arranged in a line approximately parallel to the coastline. The calibration of the vertical distance between pixels (0.766 m/px) was carried out using the suggestion of Tsuruda (2013) to use the difference in the height of the buildings and the exhaust stacks.

Sequences of images were extracted as individual files from the WMV video in BMP format and processed using the image processing suite of the MATLAB 2020b program (Mathworks, 2020). The methodology to extract the contour of the plume is illustrated in Figure 2 using an image of the explosion of Unit 3. The images are first cropped to only process the area of interest. The background of each

image is thereafter removed by calculating the absolute difference between the processed image and the image just before the explosion in RGB color scale. This step aims to increase the plume's luminosity and remove the static background. The image is binarized by threshold using the image's luminosity in the Lab color scale (first component L used). The contour is refined by applying morphological operations available in Matlab, and the contour is extracted via edge detection. The exhaust towers (Labeled S in Fig. 1) near the plume are detected by the algorithm but do not interfere with the analysis of the dispersion.

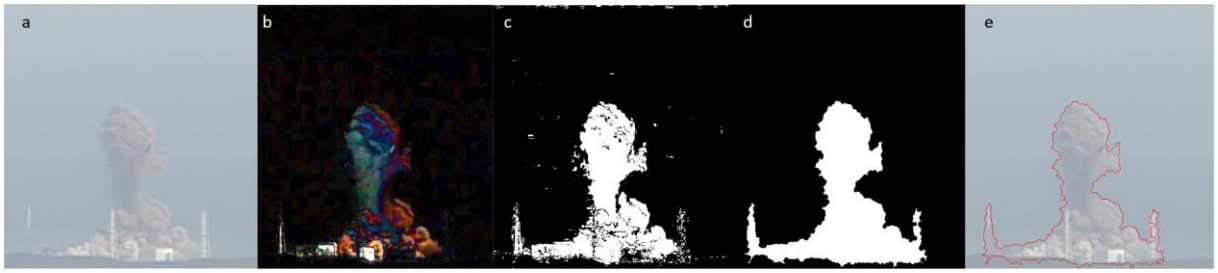

Figure 2: Image processing methodology to extract the contour of the debris plume - a) raw image, b) background removed, c) binarization by luminosity threshold, d) morphological operation, e) contour applied on the raw image

The plume contour is detected on each image, and the height of the plume, calculated using the average position of the 10% highest points in the plume contour, is extracted. The plume contour (red) and the height (blue line) are shown at different moments of the dispersion of the explosion of Unit 1 (first row) and Unit 3 (second row) in Figure 3. The clouds of debris are moving due to the initial impetus from the explosions and are subsequently carried by the wind. Interpreting the horizontal motion of debris and gas clouds is ambiguous without knowing additional information about the direction of motion. However, the vertical motion can be analyzed with reasonable accuracy.

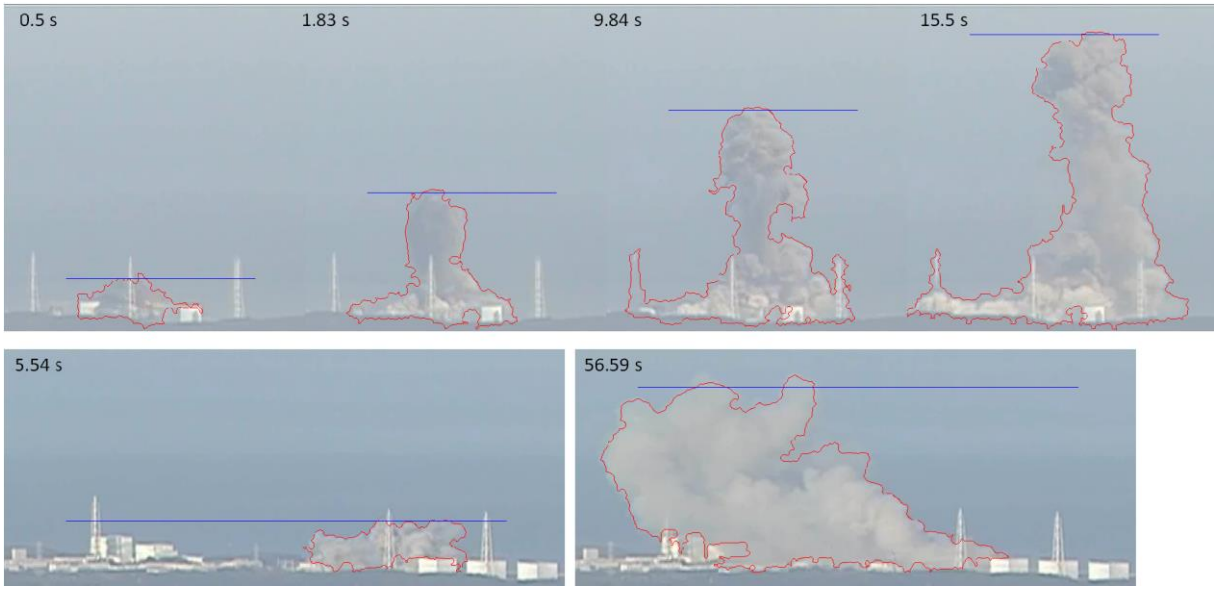

Figure 3: Contour (red) and height (blue) of the plume of the explosion of Unit 1 (top row) and Unit 3 (bottom row)

3 Analysis of the Fukushima Explosion Plumes

In our study, we examined the debris plumes of the 1F1 (Unit 1) and 1F3 (Unit 3) explosions and the condensation plume of the 1F1 explosion.

a) Debris Plumes

The variation of the plume top height is given in Figure 4 for the two explosions. The reference time (t = 0 s) is taken at the time of the first visible light on the image and the reference height (H = 0 m) is taken at the top of the reactors. The analysis stops when the video ends for the 1F1 explosion, and when the plume reaches the frame top for the 1F3 explosion.

The first observation during the analysis was the similarities between the two dispersions. Even though the 1F3 plume reaches high altitudes faster due to a potentially stronger explosion, the two dispersion plume heights superpose well once the time scale of 1F3 is multiplied by a constant value equal to 9. The overlapping curves are proposed in Figure 5. The similarity comes from the fact that the geometry of the explosion, the combustible type, and the surrounding environment are similar for the two cases, but the amount and rate of energy release differ. Scaling behavior is well established (Kinney and Graham 2013, Cao et al. 2011) for plumes and blast waves from ideal explosions of high explosives but unexpected for the highly nonideal explosions associated with gaseous combustion in a partially confining, rupturing structure.

A linear curve can be used to represent the first seconds of the two dispersions (until 9 and 2.5 seconds, for 1F1 and 1F3 respectively), typical of a ballistic motion. The linear equations are given in Figure 4. The plume generated by 1F3 rises faster and higher than the one from 1F1, implying very different energy release and release rates. The ratio of the two linear slopes corresponds to the constant value used to scale the time of the two dispersions in Figure 5.

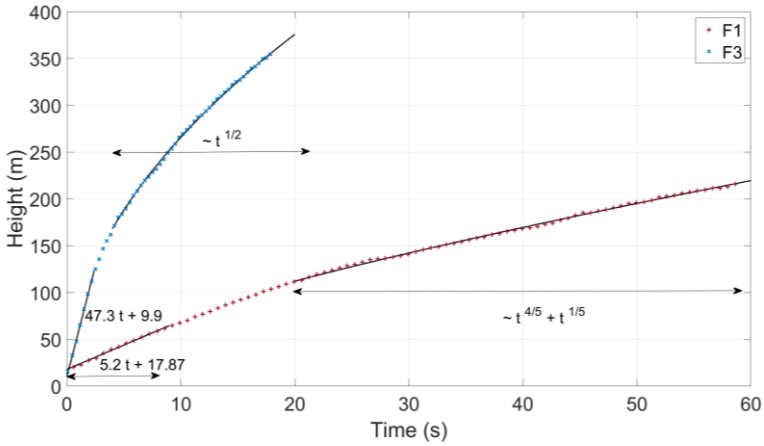

Figure 4: Debris plume height regarding time - Unit 1(+) and Unit 3 (x) explosions and linear and power fits.

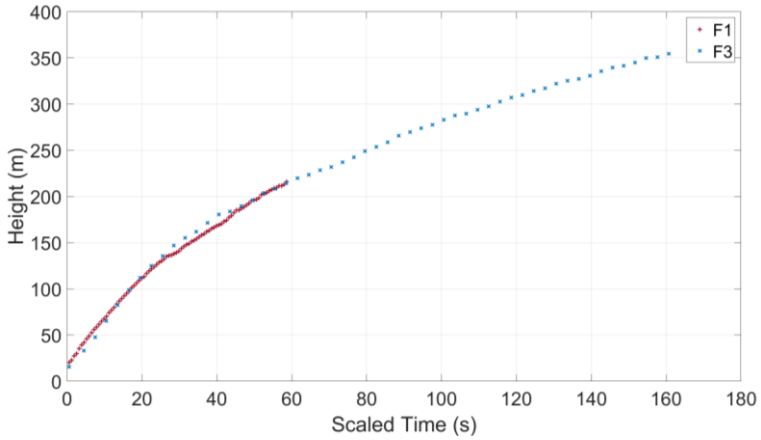

Figure 5: Similarities of Unit 1(+) and Unit 3 (x) explosions – Variation of the plume top heights, 1F3 time multiplied by 9

Although there is a rough similarity in the scaled plume height behavior for the two dispersions, differences appear with a closer look. The model recently developed by Skvortsov *et al.* (2021) for

strong convective thermals has been used to refine the analysis and get insights into the dispersions several seconds after the explosion. The model is based on the classical theories of plume rise (Turner 1973), extended to consider non-Boussinesq effects, the source mass flux, as well as buoyancy flux, factors that are significant in the Fukushima plumes. One of the key issues in modeling plumes is the rate of entrainment of the surrounding atmosphere due to fluid motion induced by the rising plume and turbulent structures in the flow. This is a source of modeling uncertainty in the integral models that are the basis of the scaling relationships.

The model proposes different power scaling laws of the centroid and the radius of the dispersion according to the predominance of buoyancy flux (thermal) or mass flux (flow) effects on the dispersion, and the density difference between the plume and the surrounding atmosphere. The power laws are summarized in Table 1. In addition to examining the plume height, the scaling laws have been tested as the sum of the radius and the centroid position variations, *i.e.*, $a.t^{\gamma} + b.t^{\delta}$, where a and b are constants determined to optimize the curve fitting, t is the time of dispersion in seconds, and γ and δ are respectively the power law for the plume centroid and the plume radius. A reasonable fit can be observed with two scaling laws. The 1F3 plume follows the first scaling law on the Table after 9 seconds of dispersion, while the 1F1 plume follows the second one after 20 seconds. The fitted equations are given in the Table. Results indicate that both plumes can be considered weak thermals, but the initial entrainment velocity of 1F1 appears dominated by buoyancy flux (thermal), while the initial entrainment of 1F3 appears dominated by mass flux (flow).

Skvortsov et al.'s models are convenient for conceptual understanding of some of the factors important to dispersion. However, because these are simplified, they do not consider other important factors that will significantly influence the dispersion, such as atmospheric stability, the atmospheric boundary layer profile, the particle density distribution in the plume, and the explosion geometry. Given the uncertainties around these factors and initial conditions for the plumes, it is challenging to go further with these simple scaling analyses.

Table 1: Scaling power laws for thermals proposed by Skvortsov et al. (2021) and application to Fukushima dispersions

Conditions	Plume Centroid	Radius	Fukushima
Weak thermal, Flow dominated	~ time $^{(1/2)}$	~ time $^{(1/2)}$	1F3 (t > 9 s) 84.06. $t^{0.5}$
Weak thermal, Thermal dominated	~ time $^{(4/5)}$	~ time $^{(1/5)}$	1F1 (t > 20 s) 6.26. $t^{4/5}$ + 23.84. $t^{1/5}$
Strong thermal, Flow Dominated	~ time $^{(2)}$	~ time $^{(4/5)}$	
Strong Thermal, Thermal dominated	~ time $^{(2)}$	~ time $^{(1/8)}$	

b) Condensation Plume

A white plume is visible at the early stage of the 1F1 explosion (between 0 and 0.3 s). This plume is suspected to be the water condensation generated by the propagation of the blast negative pressure, as observed in high explosive detonation, for example, during the Beirut explosion in 2020 (Pasman et al. 2020). The edge detection algorithm has been applied to this plume to investigate its vertical position, and a linear fit of the result leads to a mean velocity of 222 m/s. Due to the low resolution of the images, the velocity estimation can vary from 200 m/s to 280 m/s depending on the number and position of points considered (beginning, middle, or end of the plume dispersion). The literature has also found values around this speed (Tsuruda 2013). As the negative phase of a blast propagates at the speed of sound (Kinney and Graham 2013), the measured velocity supports the condensation hypothesis and the existence of a blast wave after the explosion.

4 Conclusions

Analyzing the plumes generated by the two Fukushima explosions as explosive dispersions has provided some new insights into plume behavior and potential issues in applying plume analysis to determine the characteristics of the explosions.

Even though the two plumes seem very different at first glance, similarities are observed and a time scale has been found to superpose the plume height growth curves. Using recent models for strong convective thermals, analysis of the plume rise indicates that caution is needed in interpreting the visible plumes in terms of classical thermal plume models. The scaling laws applied to the plume rise highlight that 1F1 may be initially dominated by buoyancy flux, while 1F3 plume may be initially dominated by mass flux. Both dispersions appear to be in the weak buoyancy regime several seconds after the explosion.

Substantial uncertainties exist about the Fukushima explosion that are challenging to resolve and complicate using the plumes as forensic analysis. An opportunity for future research is to obtain and analyze dispersion plume data from controlled large-scale gaseous explosions that mimic the situation encountered at Fukushima of a nonideal explosion within a failing structure.

Acknowledgment

The authors are grateful to Professor Takashi TSURUDA of Akita Prefectural University for sharing his knowledge and papers, and hosting JES visit at Akita in 2015. Yuji TERASHIMA of Fukushima Central Television kindly provided the high-resolution digital versions of the videos and information about the recordings.

References

Cao, X., G. Roy, P. Brousseau, L. Erhardt, and W. Andrews. A Cloud Rise Model for Dust and Soot from High Explosive Detonations. Propellants, Explosives, Pyrotechnics 36, no. 4 (August 2011): 303–9.

G. F. Kinney, K. J. Graham. Explosive shocks in air. Springer Science & Business Media, 2013.

Mathworks. MATLAB and Image Processing Toolbox. The Mathworks, Inc, August 2020.

NAS. Lessons Learned from the Fukushima Nuclear Accident for Improving Safety of U.S. Nuclear Plants. National Academies Press, Washington, D.C., 2014.

M. Kuznetsov, J. Yanez, J. Grune, A. Friedrich, and T. Jordan, Hydrogen combustion in a flat semi-confined layer with respect to the Fukushima Daiichi accident, Nuclear Engineering and Design, vol. 286, pp. 36–48, May 2015.

W. Luangdilok. The explosions at Fukushima Daiichi Unit 3 and Unit 4 and implications on the evaluation of 1F3 accident. Nuclear Engineering and Design, vol. 362, p. 110536, Jun. 2020.

H. Pasman, C. Fouchier, S. Park, N. Quddus, D. Laboureur. Beirut ammonium nitrate explosion: Are not we really learning anything? Process Safety Progress, vol. 39, no 4, 2020.

J. Rempe, M. Corradini, M. Farmer, J. Gabor, R. Gauntt, T. Hara, W. Luangdilok, R. Lutz, D. Luxat, S. Mizokami, K. Robb, M. Plys, K. Tateiwa, Y. Yamanaka, Safety Insights from Forensics Evaluations at Daiichi. J. Nucl. Mater. and Energy 10, 18-34, 2017.

A. Skvortsov, T. Dubois, M. Jamriska, M. Kocan. Scaling laws for extremely strong thermals. Physical Review Fluids, vol. 6, no 5, p. 053501, 2021.

Y Terahsima. Video recording of Fukushima Daiichi Explosion, Email and FTP to JE Shepherd, February 2014.

T. Tsuruda. Nuclear Power Plant Explosions at Fukushima-Daiichi. Procedia Engineering, 62:71–77, 2013.

J. S. Turner, Buoyancy Effects in Fluids. Cambridge University Press, 1973.

J. Yanez, M. Kuznetsov, and A. Souto-Iglesias, An analysis of the hydrogen explosion in Fukushima Daiichi Unit 1. International Journal of Hydrogen Energy, vol. 40, pp. 8261–8280, 2015.